Bioinspired Peptoid Nanotubes for Targeted Tumor Cell Imaging and Chemo-Photodynamic Therapy

Yanan Luo, Yang Song, Mingming Wang, Tengyue Jian, Shichao Ding, Peng Mu, Zhihao Liao, Qiurong Shi, Xiaoli Cai, Haibao Jin, Dan Du, Wen-Ji Dong, Chun-Long Chen, and Yuehe Lin**

Substantial progress has been made in applying nanotubes in biomedical applications such as bioimaging and drug delivery due to their unique architecture, characterized by very large internal surface areas and high aspect ratios. However, the biomedical applications of organic nanotubes, especially for those assembled from sequence-defined molecules, are very uncommon. In this paper, the synthesis of two new peptoid nanotubes (PepTs1 and PepTs2) is reported by using sequence-defined and ligand-tagged peptoids as building blocks. These nanotubes are highly robust due to sharing a similar structure to those of nontagged ones, and offer great potential to hold guest molecules for biomedical applications. The findings indicate that peptoid nanotubes loaded with doxorubicin drugs are promising candidates for targeted tumor cell imaging and chemo-photodynamic therapy.

Although 1D nanotubes have made success in broadly biological fields,[1] such as nanozyme-catalysis,[2] biosensing,[3] bioimaging,[4] as well as drug delivery and cancer theranostics,[5,6] the controversial cytotoxicity issue of inorganic materials (e.g., carbon nanotubes) limits their further application in biomedicine. With the development of molecular self-assembly,[7–9] an increasing number of low-toxic 1D organic nanotubes (ONTs) have been synthesized as alternatives.[10] Among these biomimetic ONTs, nanotubes by using peptides[11] as building blocks are most widely investigated. However, the biomedical applications of these peptide nanotubes are confronted with some limitations due to their intrinsic drawbacks. For instance, the functional diversity is poor because of the self-assembly of peptides relying on the natural motifs or dipeptides. Therefore, the sequence-editing or modification in peptides is unavailable.[12,13] These natural peptide-based nanotubes suffer from poor protease-resistance. To enhance their stability, nanotubes assembled by peptide amphiphiles have been synthesized. But the typical peptide amphiphiles usually consist of four regions (i.e., a hydrophobic tail, a linker, a spacer, and a hydrophilic head), which is complicated and difficult to control.[12,14] Therefore, it is highly demanded to exploit novel ONTs integrating the engineering of sequence-defined, functionalization and high stability into one system.

Peptoids are now attracting increasing attention in a variety of fields due to several distinct advantages, such as low cost, easy synthesis, good biocompatibility, and versatile side-chain chemistry. As peptide-mimetics, peptoids are sequence-specific heteropolymers containing rich information and possess the advantages of both biopolymers and synthetic polymers. The sequential N-substituted glycine units cause peptoids to fold into diverse, defined structures,[15–17] lacking chirality or hydrogen bonds.[18–20] It is worth noting that N-substitution greatly improves the peptidase/proteinase-resistance of peptoids, as well as their chemical and thermal stability.[21] The enhanced stability of peptoids is thought to prevent a premature drug release caused by enzymatic degradation.[22] Additionally, compared with nanostructures in other morphologies, nanotubes as drug nanocarriers have been reported to have a longer persistence in blood.[23] All these features promote peptoid-based nanotubes as ideal nanocarriers for tumor intracellular imaging, drug delivery and cancer therapy. Unfortunately, the biomedical applications of 1D ONTs are still at the infant stage.[24–27]

We recently reported a new class of highly engineered and dynamic nanotubes by assembling sequence-defined peptoids through a unique "rolling-up and closure of nanosheet" process. Due to the large side-chain diversity of peptoids, these nanotubes can be easily engineered with a broad range of functional groups.[28] Herein, as a proof-of concept of assembling

Dr. Y. Luo, Dr. Y. Song, S. Ding, Dr. Q. Shi, Dr. X. Cai, Prof. D. Du, Prof. Y. Lin
School of Mechanical and Materials Engineering
Washington State University
Pullman, WA 99164, USA
E-mail: yuehe.lin@wsu.edu

Dr. M. Wang, T. Jian, P. Mu, Z. Liao, Dr. H. Jin, Prof. C.-L. Chen
Physical Sciences Division
Pacific Northwest National Laboratory
Richland, WA 99352, USA
E-mail: chunlong.chen@pnnl.gov

Prof. W.-J. Dong
Chemical Engineering and Bioengineering
Washington State University
Pullman, WA 99164, USA

Prof. C.-L. Chen
Department of Chemical Engineering
University of Washington
Washington 98195, USA
E-mail: chen881@uw.edu

functional nanotubes for biomedical applications, we synthesized two new functional peptoid nanotubes (PepTs1 and PepTs2) by coassembling ligand-tagged tube-forming peptoids that contain folic acid (FA), dansyl (DNS), and meso-tetrakis (4-carboxylphenyl)porphyrin (TCPP) (Figures S1–S3, Supporting Information). We demonstrated the applications of these nanotubes in drug delivery and multimodal cancer cell therapy.

Ligand-tagged peptoids (**Figure 1**a) were synthesized using a previously developed submonomer synthesis method (see the Supporting Information for details), in which functional groups FA, DNS, and TCPP were covalently attached at the N-terminus of peptoids.[16,28,29] Among these functional ligands, FA is known as an efficient t argeting l igand t hat s pecifically re cognizes FA receptors-overexpressed cells.[30] DNS dye was chosen because it can be easily built into tube-forming peptoids and has bright green fluorescence after reaction with primary amino groups.[31] TCPP is a well-known commercially available photosensitizers used in photodynamic therapy (PDT).[32] To develop functional nanotubes that are suitable for targeted imaging and for PDT, FA-tagged peptoids (Pep-FA) were coassembled with Pep-DNS or Pep-TCPP in a molar ratio of 1:1, respectively (see the Supporting Information for details). Nanotubes assembled from Pep-FA and Pep-DNS (PepTs1) were further loaded with antitumor drug doxorubicin (DOX) for drug delivery and monitoring the intracellular drug release (**Figure 2**a). PepTs1 exhibited an extraordinary drug holding capacity. Nanotubes assembled from Pep-FA and Pep-TCPP (PepTs2) were further loaded with DOX to proceed a chemo-photodynamic therapy. To the best of our knowledge, it is the first time that nanostructures formed by peptoids have been implemented in targeted cancer cell imaging and therapy.

As shown in Figure 1 and Figure S4 (Supporting Information), both transmission electron microscopy (TEM) and atomic force microscopy (AFM) images showed that the coassembly of two functional peptoids led to the formation of PepTs1 and PepTs2 with well-defined tubular structures, in which PepTs1 has a wall thickness of 3.41 nm (analysis with ImageJ). When Pep-TCPP was used for coassembly with Pep-FA instead of Pep-DNS, the formed nanotubes exhibited a slightly larger wall thickness of 3.51 nm, which can be seen from the negatively stained TEM images in Figure 1b. The increased wall thickness of PepTs2 is due to the large size of TCPP, ≈18 Å.[33] Both of PepTs1 and PepTs2 possessed larger wall thickness than our earlier reported $Nbpm_6Nce_6$ nanotubes,[28] indicating that the ligand-tails were involved in the increase of tube wall thickness. The AFM image shows the heights of PepTs1 and PepTs2 are 6.82 and 6.93 nm, respectively, nearly two times of their wall thickness (Figure 1c and Figure S4, Supporting Information). To elucidate the assembly pathway, we collected the morphologies of PepTs1 at the different stages by AFM (Figure S5, Supporting Information). In order to use PepTs1 and PepTs2 for cellular experiments, colloidal nanotubes with nanoscale length were obtained by a sonication-assisted tube-cutting process (see the Supporting Information for details). The TEM image of the PepTs2 showed that the sonication treatment shortened the length of PepTs2 while the tube wall thickness remained unchanged (Figure 1d). The dynamic light scattering (DLS, Figure 1e) data of the colloidal PepTs2 show that they have an average length of ≈298.8 nm. The X-ray diffraction (XRD) data of PepTs2 (Figure 1f) and of PepTs1 (Figure S6, Supporting Information) shows that these functional nanotubes are highly crystalline and exhibit a similar framework structure of our previously reported nonlabeled peptoid nanotubes.[28] Additionally, the stability of PepTs1 and PepTs2 in PBS buffer 1X and F-12K medium containing 10% FBS or treated with 50 °C for 6 h were tested, respectively. As expected, both of PepTs1 and PepTs2 maintained their tubular structure, reflecting the highly stable nature (Figure S7, Supporting Information).

Figure S8A (Supporting Information) shows that PepTs2 exhibits a strong UV absorption at the wavelength of 419 nm and nanotubes without TCPP functional groups have no obvious absorbance in the visible-light region. Besides, because TCPP is also known as a fluorescent reagent, the fluorescent properties of PepTs2 were also characterized. As shown in Figure S8B (Supporting Information), the fluorescence emission spectrum of PepTs2 shows a peak at 660 nm with an excitation wavelength of 415 nm, which belongs to the fluorescence emission of TCPP. The strong UV absorbance at 419 nm and fluorescence emission at 660 nm suggested the optical properties of TCPP were retained after the formation of functional nanotubes. Subsequently, the cellular selectivity of nanotubes was investigated by incubating PepTs2 with FA receptor overexpressed H1299 cells and negatively expressed A549 cells, respectively. After incubating for 1 h, a strong red fluorescence signal coming from TCPP was observed in H1299 cells, while there was almost no such fluorescence signal seen in A549 cells (Figure 2b). These results indicated that the prepared PepTs2 exhibited an effective targeting on FA receptor-overexpressed H1299 cells due to the highly specific recognitions between FA and FA receptor and the selectively cellular internalization of nanotubes. To verify the internalization process to be an endocytosis pathway, transferritin-488 Alexa Fluor (Tf-488), which is well-known to undergo receptor-mediated endocytosis,[34] was coincubated with the cells. Figure 2c shows the 3D Z stack confocal laser scanning microscopy (CLSM) image of H1299 cells by the fluorescence colocalization of Tf-488 and PepTs2. After incubation for 1 h, the endosomes in H1299 cells were stained by Tf-488 with green fluorescence. Then the green fluorescence of Tf-488 and the red fluorescence of PepTs2 contribute to a yellow color in the overlap image, indicating that PepTs2 mainly distributed in the endosomes due to the FA-mediated endocytosis pathway. Figures S9 and S10 (Supporting Information) show the orthogonal images of H1299 cells and A549 cells after incubation with PepTs2, respectively. Corresponding to the results above, the overlapping yellow signal can be only observed in H1299 cells, but not in A549 cells.

Before applying PepTs1 for intracellular bioimaging, their compatibility was first evaluated by incubating them with H1299 cells for 4 h. Since actin and microtubulin play irreplaceable roles in the construction and preserving the integrity of cytoskeleton,[35] the morphology changes of F-actin and microtubules in cells treated with PepTs1 were observed. As in Figures S11A,B (Supporting Information), the microtubules (white color) and actin filaments (stained in red) extended through the entirety of these cells. The cells remained intact and the cytoskeleton of H1299 cells was not disrupted, indicating that the PepTs1 tubes have no effect on the activities of cells. Additionally, the cell viability of H1299 after incubation with PepTs1 was evaluated by 3-(4,5-dimethylthiahiazo-2-yl)-2,5-di-phenytetrazoliumromide (MTT) assays. As shown in Figure S11C

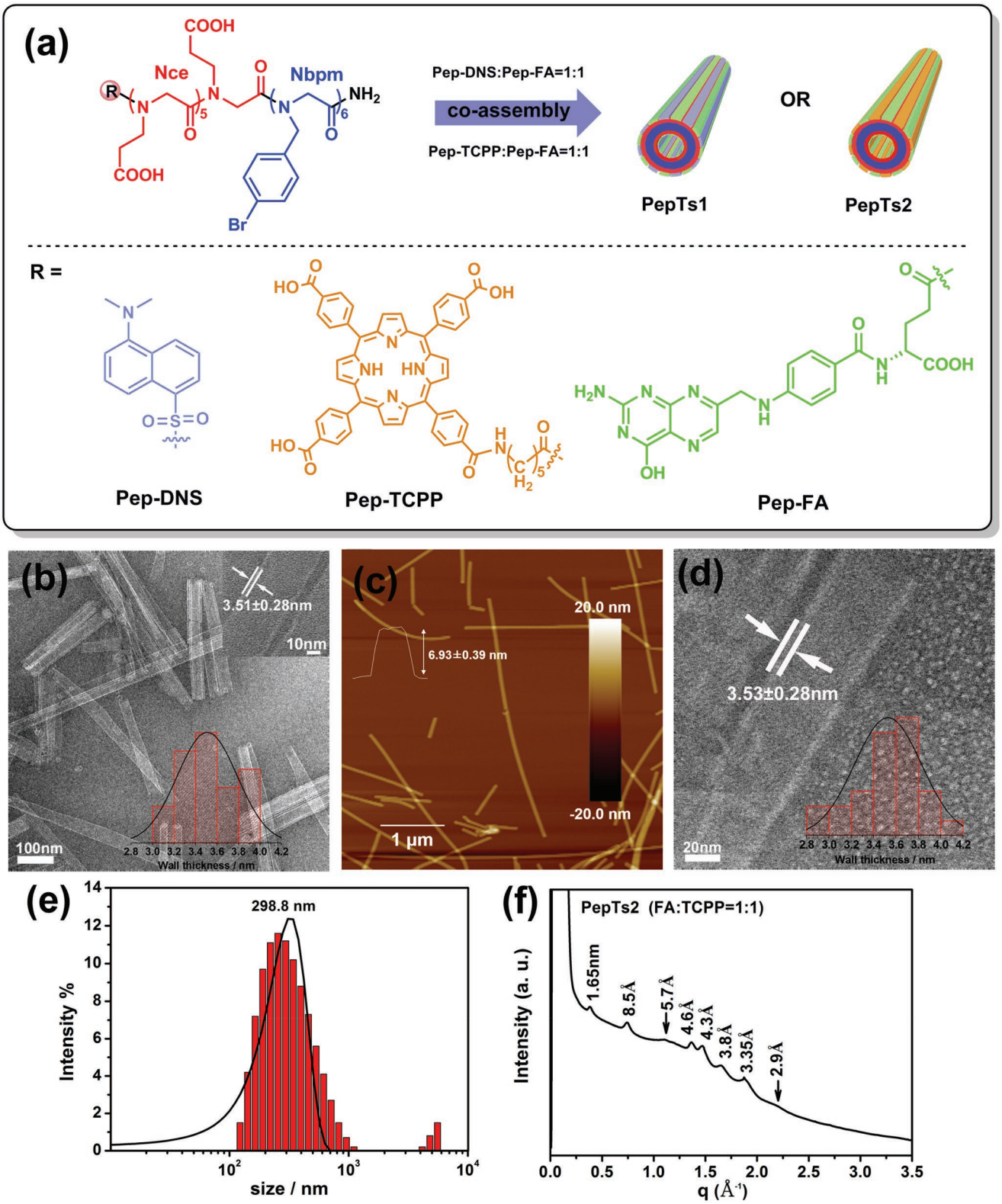

Figure 1. a) The structures of ligand-tagged $Nbpm_6Nce_6$ peptoid sequences and the assembly of them into 1D tubes. -R represents -Nc_6TCPP, -DNS, and -FA, respectively. PepTs1 formed by Pep-FA coassembled with Pep-DNS at a ratio of 1:1. PepTs2 formed by Pep-FA coassembled with Pep-TCPP at a ratio of 1:1. b) TEM images of PepTs2. c) AFM image of PepTs2. d) TEM image of PepTs2 after sonication. e) Dynamic light scattering (DLS) data of PepTs2 showing the average tube length is about 298.8 nm after sonication. f) XRD spectrum of PepTs2 after sonication, the values of each peak is obtained by a conversion based on the equation of $d = 2\pi/q$.

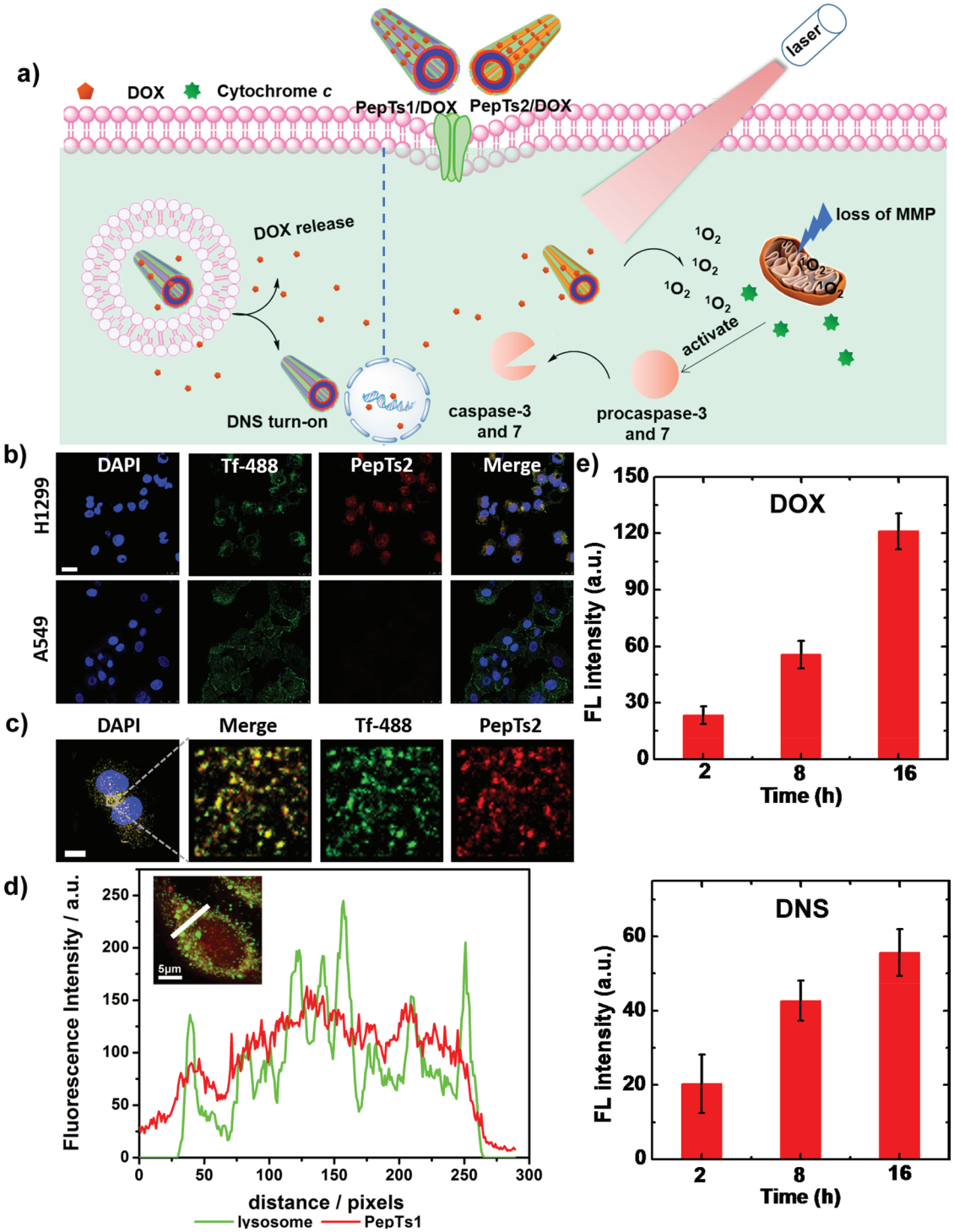

Figure 2. a) The endocytosis process of PepTs1 as platform to deliver DOX to H1299 cells, and activation of the apoptosis pathway caused by PepTs2 in H1299 cells. b) Targeting intracellular uptake of PepTs2 against H1299 cells and A549 cells. c) Z stack colocalization image of Tf-488 and PepTs2 in H1299 cells. d) Spatial-intensity profile of H1299 cell along the white line. e) The fluorescence intensity analysis of DOX and DNS for drug release monitoring.

(Supporting Information), more than 85% of cells survived even when PepTs1 concentration was as high as 80×10^{-6} M, indicating the low cytotoxicity of PepTs1. DNS is a molecule that has a bright green fluorescence emission after being conjugated with the N-terminal of peptides. Thus, PepTs1 with green fluorescence was then incubated with H1299 cells to investigate the post endocytosis distribution of PepTs. H1299 cells were treated with PepTs1 for 4 h and followed by staining with LysoTracker.

As seen from the confocal imaging (Figure S12, Supporting Information), the lysosomes of H1299 cells emit bright red fluorescence, which has a good overlap of the green fluorescence from PepTs1. Additionally, intracellularly fluorescence quantitative colocalization analysis of the lysosomal compartments and PepTs1 was further performed by calculating the Pearson correlation coefficient.[36] The weighted colocalization coefficient was determined to be 72% (n = 20 cells; Figure 2d). These results suggested that most of the PepTs1 tubes went through an early endosome to late endosome pathway and finally were trapped in lysosomal compartments. Also, the drug delivery ability of PepTs was evaluated by DOX-loading PepTs1/DOX. DOX was absorbed onto the PepTs1 by π–π stacking and the drug loading efficiency was calculated to be 30.05% (Figure S13, Supporting Information). However, the fluorescence of both DOX and DNS diminished after loading DOX onto PepTs1 (data not shown). We hypothesized that the intermolecular distance between DOX and DNS was less than 100 Å, resulting in Förster resonance energy transfer (FRET) and fluorescence quenching. The time-dependent drug release profile of DOX was recorded by redispersed PepTs1/DOX in pH 5.5 acetate buffer solution and pH 7.4 PBS. As shown in Figure S14B (Supporting Information), DOX showed an increased release with the increase of incubation time, and ≈40% of the DOX was released in pH 5.5 solution after 12 h. The release profile of DOX indicated that PepTs1/DOX had an acid-responsive drug release and could be further applied to investigate the intracellular drug delivery in H1299 cells, which have a weakly acidic environment. Visualization of the DOX-releasing process was validated by confocal imaging based on the quenching effect. Time-dependent fluorescence recovery of both DOX and DNS was observed after incubating PepTs1/DOX with H1299 cells for different times (Figure S14A, Supporting Information). After incubation for 2 h, only slightly red and green fluorescence can be observed. In this process, PepTs1/DOX went through endocytosis and lysosomal trap, followed by DOX releasing from PepTs1. Prolonging the incubation time to 8 h, much brighter red and green fluorescence were observed due to more PepTs1/DOX entering the cells and more DOX released. After incubation for 16 h, most of DOX located in the nuclei and thus induced the cell apoptosis, while the PepTs1 mainly distributed in the cytoplasm. The corresponding fluorescence intensity of DOX and DNS at 2, 8, and 16 h were recorded, respectively (Figure 2e).

Photodynamic therapy is known as a noninvasive approach to treat cancer by producing amounts of harmful single oxygen ($^1O_2$) with the activation of light. The level of $^1O_2$ is the essential factor in the PDT process and dominates the efficacy of PDT. The challenge is that most of the reported photosensitizers are highly hydrophobic with poor solubility, which limits their application efficiency in cancer therapy.[37,38] Much effort has been dedicated to improving the solubility of photosensitizers in physiological fluids by loading or encapsulating them into biocompatible nanocarriers.[39] The precise attachment of TCPP to peptoid oligomers and self-assembly them into crystalline nanotubes not only provide the accessibility of hydrophobic TCPP in physiological fluid, but also avoid the possible self-aggregation caused by the close proximity between TCPP molecules.[40] The ability of PepTs2 to produce single oxygen ($^1O_2$) in vitro was assessed by monitoring the absorption of 1,3-diphenylisobenzofuran (DPBF), which causes an absorbance loss by the oxidation reaction of $^1O_2$. As shown in Figure S15A (Supporting Information), the absorbance of DPBF dispersed in PepTs2 solution decreased dramatically with the increase of irradiation time. Also, a concentration-dependent decrease of absorbance for DPBF in PepTs2 solution with concentration varying from 25 to 87.5 × 10^{-6} M was observed under irradiation (Figure S15C, Supporting Information). As a control, the absorbance of DPBF in PBS kept almost no changes after exposed to irradiation for 10 min (Figure S15B, Supporting Information). The UV absorbance loss of DPBF at 410 nm in different solutions upon 660 nm laser irradiation was converted and shown in **Figure 3**a. Both free TCPP and PepTs2 that contains precisely arranged TCPPs resulted in the most significant absorbance loss of DPBF, indicating the continuous generation of $^1O_2$. Compared with the unchanged UV absorbance of DPBF in PBS, these results indicated that the $^1O_2$ was generated by TCPP and the conjugation of TCPP to peptoids with tube-like formation well preserved the photochemical properties of TCPP. Interestingly, the UV absorbance loss of DPBF decreased significantly in the presence of ascorbic acid (AA), which acts as $^1O_2$ scavengers. The inhibition of AA to the generation of $^1O_2$ verified that the UV absorbance loss of DPBF was caused by the $^1O_2$. Additionally, the singlet oxygen quantum yield of Pep-TCPP and PepTs2 have been calculated by using methylene blue as reference, respectively (Figure S16, Supporting Information). $\Phi_{Pep\text{-}TCPP}$ was 0.522, and Φ_{PepTs2} was 0.17. The decrease value of Φ_{PepTs2} probably due to the π–π stacking of TCPP in the process of assembly. Subsequently, the intracellular generation of $^1O_2$ was detected with the indicator 2′,7′-dichlorofluorescin diacetate (DCFH-DA) for confocal imaging. The cell-permeable DCFH-DA molecules are known to have strong green fluorescence emission when they undergo de-esterification and oxidation. As shown in Figure 3b, the fluorescence signal could hardly be observed when the H1299 cells were incubated with PepTs2 for 4 h, indicating that no $^1O_2$ was generated. After exposed to 660 nm laser irradiation, the indicator in H1299 cells emitted strong green fluorescence, indicating a large amount of $^1O_2$ generation. Corresponding to the results of tests in vitro, the fluorescence intensity of H1299 cells decreased dramatically when coincubated with PepTs2 and AA. All the results above indicated that PepTs2 nanotubes with precisely displayed TCPPs were able to produce $^1O_2$ effectively both in vitro and intracellularly.

After verifying the ability to generate $^1O_2$, the biological effect of PepTs2 was assessed. The integrity of mitochondria that can be assessed by mitochondrial membrane potential (MMP) was first examined by using the MMP indicator rhodamine 123 (Rho 123).[41] In normal cells, Rho 123 molecules penetrate and accumulate in the mitochondria relying on MMP, accompanied by the decrease or diminish of fluorescence. The collapse of MMP induces the release of Rho 123 to the cytoplasm and results in a recovery of fluorescence. As shown in Figure 3c, H1299 cells containing Rho 123 emit bright red fluorescence after incubation with PepTs2 for 4 h and irradiation treatment. That was because the $^1O_2$ generated by PepTs2 inside the cells disrupted the integrity of mitochondria, followed by the collapse of MMP and release of Rho 123. As a negative control, the cells without irradiation exhibited negligible fluorescence

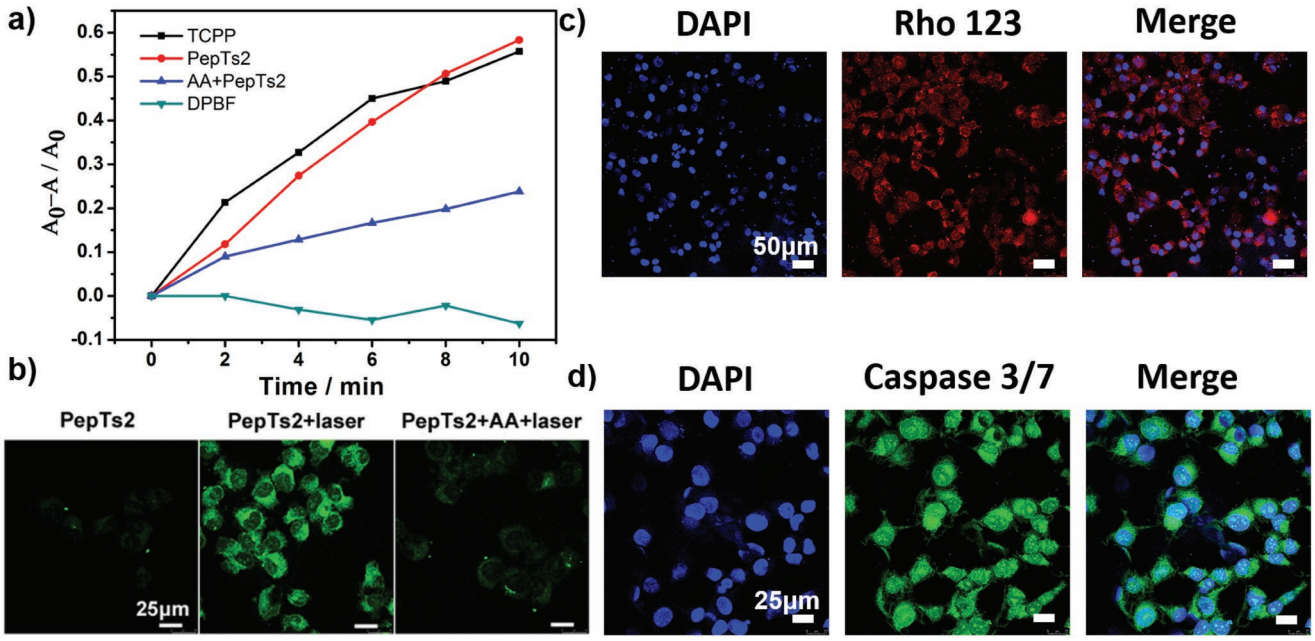

Figure 3. a) The UV absorbance loss of DPBF in TCPP, PepTs2, PepTs2 containing 50×10^{-6} M AA solution and PBS, respectively, under 660 nm laser irradiation at a power of 50 mW cm^{-2}. b) The intracellular generation of singlet oxygen in H1299 cells treated with 1.25×10^{-6} M PepTs2. The laser irradiation power was 660 nm 50 mW cm^{-2} for 5 min. c) Rho 123 and d) caspase 3/7 kit stained H1299 cells after incubation with 2.5×10^{-6} M PepTs2 and irradiation for 5 min. The laser power was 50 mW cm^{-2}.

signal (Figure S17, Supporting Information). Additionally, the cells with irradiation but pretreated with 100×10^{-6} M FA also showed a weak fluorescence signal, which could be attributed to the inefficient internalization of PepTs2. It has been reported by other researchers that significant loss of MMP is involved in cell apoptosis through the release of cytochrome c from the mitochondria and activation of the caspase-dependent apoptosis pathway.[42–44] Thus, a luminescent assay was conducted to assess the activities of caspase 3/7. The caspase 3/7 substrate is cleaved to produce the luminescent product by caspase cleavage. H1299 cells containing PepTs2 were stained with a caspase 3/7 kit after irradiation treatment. As expected, strong green fluorescence was observed in the cells, representing the activation of caspase 3/7. In contrast, H1299 cells without irradiation and FA-negatively expressed A549 cells showed weak green fluorescence (Figure S18, Supporting Information). These phenomena illustrated that the intracellular generation of $^1O_2$ contributed to the enhanced activities of caspase 3/7 and activation of apoptosis signal.

To verify the phototoxicity of PepTs2 against the cells, live/dead cell double staining kit (propidium iodide, PI/calcein-AM) was used. Calcein-AM is highly lipophilic and can easily penetrate into the living cell membrane to generate strong green fluorescence emission, while PI can only stain dead cells to give a bright red fluorescence emission. As shown in **Figure 4**a, almost all the cells containing PepTs2 without irradiation kept high activities due to the absence of cytotoxic $^1O_2$. Upon exposed to irradiation at 660 nm, most of the cells containing PepTs2 died. Additionally, most of the cells pretreated with FA remained alive though exposed to irradiation because of the inefficient internalization of PepTs2. Finally, the chemo-photodynamic dual-modal therapy efficiency of PepTs against H1299 cells was evaluated by MTT assays by incubation them with DOX-loading PepTs2 (PepTs2/DOX). The biocompatibility of PepTs2 was evaluated by incubating H1299 cells and A549 cells with PepTs2 at different concentrations for 24 h, respectively. As shown in Figure S19A (Supporting Information), both of the H1299 cells and A549 cells survived, indicating that PepTs2 is nontoxic to the cells without the activation of laser irradiation. Upon exposed to irradiation, the viability of H1299 cells tended to decrease with the increasing concentrations of PepTs2, while that of A549 cells was higher than 80% (Figure S19B, Supporting Information). That is due to the inefficient internalization of PepTs2 by A549 cells, resulting in the insufficient generation of $^1O_2$. The different viability between A549 and H1299 cells demonstrated the ability of PepTs2 to selectively kill H1299 cells under irradiation. Impressively, the cell viability of H1299 cells decreased dramatically when they were incubated with PepTs2/DOX and with irradiation treatment (Figure 4b). Over 50% of the cells were killed at a very low concentration of PepTs2/DOX, which was much higher than the cells treated with single chemotherapy or PDT. This result may be a combined killing effect due to the combination of the chemotherapy potential of DOX and PDT of PepTs2.

In summary, by attaching functional groups, including -TCPP, -FA, and -DNS into the tube-forming peptoids and coassembling them with a molar ratio of 1:1, we successfully synthesized nanotubes with precisely controlled functional groups for targeted tumor cell imaging and chemo-photodynamic therapy. The as-prepared peptoid nanotubes exhibited good biocompatibility to the cells. Furthermore, peptoid nanotubes containing FA ligands showed high selectivity to the H1299 lung cancer cells and underwent a FA-mediated endocytosis pathway. These functionalized nanotubes were shown to work well in the

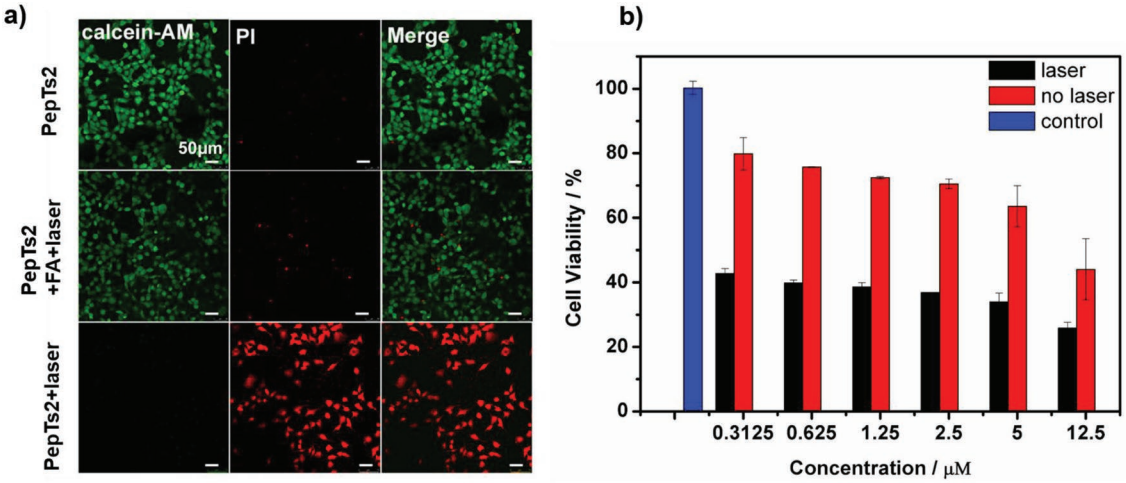

Figure 4. Phototoxicity assessment of PepTs2 against H1299 cells. a) live/dead cell images by PI/ calcein AM double staining. The laser irradiation power was 660 nm 500 mW cm^{-2} for 2 min. b) MTT assay of the cytotoxicity of PepTs2/DOX against H1299 cells with/without irradiation at power of 500 mW cm^{-2} for 5 min.

following applications: i) PepTs1 had high drug loading efficiency and showed time-dependent, sustainable DOX release in pH 5.5 acidic environment; ii) PepTs2 addressed the hydrophobicity problem of TCPP, and preserved their ability to effectively produce cytotoxic $^1O_2$. Additionally, MTT results showed that DOX-loading PepTs2 have high killing efficiency toward H1299 cells due to the combined chemo- photodynamic therapy.

Experimental Section

Peptoids Synthesis and the Self-Assembly of Peptoid Nanotubes: The pepoid oligomers were synthesized using a solid-phase submonomer method on a commercial Aapptec Apex 396 robotic synthesizer. The details are described in the Supporting Information.

Targeting Cellular Uptake of Peptoid Nanotubes: H1299 cells and A549 cells were seeded in 12-well plate at a density of 1×10^5 cells per well overnight. The cells were then incubated with Tf-488 at a concentration of 5 μg mL^{-1} for 1 h, followed by adding 1.25×10^{-6} M PepTs2 and incubation for another 1 h.

DOX Loading and Release: Dox loading was performed by gently mix DOX and PepTs1, PepTs2 aqueous solution for 12 h and centrifugation, respectively. The extracellular DOX release was carried out by dialysis PepTs1/DOX, PepTs2/DOX in pH 5.5 acetate solution. For the intracellular DOX release, H1299 cells were incubated with PepTs1/DOX for 2, 8, and 16 h, respectively. The cells were fixed and stained with DAPI for CLSM imaging.

The loading efficiency was further calculated by the equation

$$\text{Loading efficiency}\,(\%) = \frac{\text{weight of loaded drug}}{\text{total weight of peptoid nanotubes}} \times 100 \quad (1)$$

Singlet Oxygen Detection In Vitro: For extracellular detection, the DPBF was pre-mixed with the sample solution (free TCPP, PepTs2, PepTs2 with AA, PBS) at a concentration of 100×10^{-6} M, then the cells were exposed to 660 nm laser irradiation at a power density of 50 mW cm^{-2}. The absorption of DPBF at 410 nm was recorded with a microplate reader at an interval of 2 min.

For intracellular detection, H1299 cells were incubated with PepTs2 for 4 h, followed by incubating with 10×10^{-6} M DCFH-DA for 30 min. DCFH-DA containing 50×10^{-6} M AA was used as negative control. CLSM scanning was performed immediately after exposing the cells to 660 nm laser irradiation at a power density of 50 mW cm^{-2} for 5 min.

The Calculation of Singlet Oxygen Quantum Yield: The quantum yield of singlet oxygen of nanotube (PepTs2) and monomer (Pep-TCPP) have been calculated by following the reported chemical methods. Methylene blue was used as standard reference. The calculation equation is as following

$$\varnothing_{PS} = \varnothing_{MB} \frac{K_{PS} * A_{MB}}{K_{MB} * A_{PS}} \quad (2)$$

In which, K_{PS} and K_{MB} are the decomposition rate constants of DPBF by PepTs2 (or Pep-TCPP) and MB. A_{PS} and A_{MB} represent the light absorbed by PepTs2 (or Pep-TCPP) and MB, which are determined by integration of the absorption bands in the wavelength range of 400–700 nm. ϕ_{MB} is the singlet oxygen quantum yield of MB, which is 0.52 in water.[45]

Assay of Mitochondrial Membrane Potential and Activities of Caspase 3/7: H1299 cells were seeded in 12-well plate at a density of 1×10^5 cells per well overnight. Then the cells were incubation with PepTs2 for 4 h. H1299 cells pretreated with 100×10^{-6} M FA and A549 cells were set as a negative control. Subsequently, the cells were exposed to 660 nm laser irradiation at a power density of 50 mW cm^{-2} for 5 min. After another 4 h, rhodamine 123 (2×10^{-6} M) or two drops of caspase 3/7 kit were added to each well and incubation for 30 min for CLSM imaging.

Phototoxicity Assessment of PepTs2: H1299 cells were seeded in 12-well plate at a density of 2×10^5 cells per well and incubated overnight. Then the cells were incubated with PepTs2 for 4 h and exposed to 660 nm laser irradiation at a power density of 500 mW cm^{-2} for 5 min. After another 4 h, the cells were stained with Calcein-AM (2×10^{-6} M) and PI solution (4×10^{-6} M) in medium and incubated for 30 min. Finally, the cells were immediately visualized by CLSM with the excitation lasers at 488 and 543 nm, respectively.

For MTT assay, H1299 cells and A549 cells were seeded in 96-well plate at a density of 5000 cells per well and incubated overnight, respectively. The cells were then incubated with PepTs2 and PepTs2/DOX for 4 h with different concentrations (0.3125, 0.625, 1.25, 2.5, 5, and 12.5×10^{-6} M), followed by irradiated with 660 nm laser at a power of 500 mW cm^{-2} for 5 min and further incubation for another 24 h. Then 10 μL of MTT kit was added to each well following the kit manual. The absorbance was recorded at 570 nm with a microplate reader.

Supporting Information

Supporting Information is available from the Wiley Online Library or from the author.

Acknowledgements

Y.L. and Y.S. contributed equally to this work. Y.L. and C.-L.C. conceived and directed the project. Y.L. and Y.S. performed most of the cellular experiments and data analysis, and wrote the manuscript. M.W., T.J., P.M., Z.L., and H.J., performed the synthesis, self-assembly of amphiphilic peptoid oligomers and characterizations of materials. S.D. performed the drug loading test and singlet oxygen quantum yield tests. Q.S. and X.C. made the scheme draft. W.-J.D. and D.D. revised the manuscript. All authors read and commented on the manuscript. This work was supported by start-up funds from Washington State University. Peptoid synthesis work was supported by the Materials Synthesis and Simulation Across Scales (MS3) Initiative through the LDRD fund at Pacific Northwest National Laboratory (PNNL). Assembly of peptoid nanotubes and their structural characterizations were supported by the U.S. Department of Energy, Office of Basic Energy Sciences, Biomolecular Materials Program at PNNL. Production and characterization of sonication-cut nanotubes was supported by the US Department of Energy, Office of Science, Office of Basic Energy Sciences, as part of the Energy Frontier Research Centers program: CSSAS—The Center for the Science of Synthesis Across Scales under Award Number DE-SC0019288. XRD work was conducted at the Advanced Light Source with support from the Molecular Foundry, at Lawrence Berkeley National Laboratory, both of which are supported by the Office of Science, under contract No. DE-AC02-05CH11231. PNNL is a multi-program national laboratory operated for the Department of Energy by Battelle under Contract No. DE-AC05-76RL01830.

Conflict of Interest

The authors declare no conflict of interest.

Keywords

chemo-/photodynamic therapy, peptoids nanotube, singlet oxygen, targeted drug delivery

Received: May 15, 2019
Revised: August 11, 2019

[1] T. Shimizu, H. Minamikawa, M. Kogiso, M. Aoyagi, N. Kameta, W. Ding, M. Masuda, *Polym. J.* **2014**, *46*, 831.
[2] Q. Shi, Y. Song, C. Zhu, H. Yang, D. Du, Y. Lin, *ACS Appl. Mater. Interfaces* **2015**, *7*, 24288.
[3] R. de la Rica, E. Mendoza, L. M. Lechuga, H. Matsui, *Angew. Chem., Int. Ed.* **2008**, *47*, 9752.
[4] Q. Lu, D. Ericson, Y. Song, C. Zhu, R. Ye, S. Liu, J. A. Spernyak, D. Du, H. Li, Y. Wu; Y. Lin, *ACS Appl. Mater. Interfaces* **2017**, *9*, 23325.
[5] A. Bianco, K. Kostarelos, M. Prato, *Curr. Opin. Chem. Biol.* **2005**, *9*, 674.
[6] Z. Liu, S. Tabakman, K. Welsher, H. Dai, *Nano Res.* **2009**, *2*, 85.
[7] J. Song, R. Xing, T. Jiao, Q. Peng, C. Yuan, H. Möhwald, X. Yan, *ACS Appl. Mater. Interfaces* **2018**, *10*, 2368.
[8] R. Zhang, R. Xing, T. Jiao, K. Ma, C. Chen, G. Ma, X. Yan, *ACS Appl. Mater. Interfaces* **2016**, *8*, 13262.
[9] R. Xing, K. Liu, T. Jiao, N. Zhang, K. Ma, R. Zhang, Q. Zou, G. Ma, X. Yan, *Adv. Mater.* **2016**, *28*, 3669.
[10] T. Shimizu, M. Masuda, H. Minamikawa, *Chem. Rev.* **2005**, *105*, 1401.
[11] J. D. Hartgerink, J. R. Granja, R. A. Milligan, M. R. Ghadiri, *J. Am. Chem. Soc.* **1996**, *118*, 43.
[12] N. Habibi, N. Kamaly, A. Memic, H. Shafiee, *Nano Today* **2016**, *11*, 41.
[13] L. Adler-Abramovich, P. Marco, Z. A. Arnon, R. C. G. Creasey, T. C. T. Michaels, A. Levin, D. J. Scurr, C. J. Roberts, T. P. J. Knowles, S. J. B. Tendler, E. Gazit, *ACS Nano* **2016**, *10*, 7436.
[14] H. Zhu, H. Wang, B. Shi, L. Shangguan, W. Tong, G. Yu, Z. Mao, F. Huang, *Nat. Commun.* **2019**, *10*, 2412.
[15] J. Sun, X. Jiang, R. Lund, K. H. Downing, N. P. Balsara, R. N. Zuckermann, *Proc. Natl. Acad. Sci. USA* **2016**, *113*, 3954.
[16] H. Jin, F. Jiao, M. D. Daily, Y. Chen, F. Yan, Y. H. Ding, X. Zhang, E. J. Robertson, M. D. Baer, C. L. Chen, *Nat. Commun.* **2016**, *7*, 12252.
[17] F. Jiao, Y. Chen, H. Jin, P. He, C.-L. Chen, J. J. De Yoreo, *Adv. Funct. Mater.* **2016**, *26*, 8960.
[18] R. J. Simon, R. S. Kania, R. N. Zuckermann, V. D. Huebner, D. A. Jewell, S. Banville, S. Ng, L. Wang, S. Rosenberg, C. K. Marlowe, *Proc. Natl. Acad. Sci. USA* **1992**, *89*, 9367.
[19] K. T. Nam, S. A. Shelby, P. H. Choi, A. B. Marciel, R. Chen, L. Tan, T. K. Chu, R. A. Mesch, B. C. Lee, M. D. Connolly, C. Kisielowski, R. N. Zuckermann, *Nat. Mater.* **2010**, *9*, 454.
[20] R. V. Mannige, T. K. Haxton, C. Proulx, E. J. Robertson, A. Battigelli, G. L. Butterfoss, R. N. Zuckermann, S. Whitelam, *Nature* **2015**, *526*, 415.
[21] J. Sun, R. N. Zuckermann, *ACS Nano* **2013**, *7*, 4715.
[22] Y. Song, M. Wang, S. Li, H. Jin, X. Cai, D. Du, H. Li, C.-L. Chen, Y. Lin, *Small* **2018**, *14*, 1803544.
[23] Y. Geng, P. Dalhaimer, S. Cai, R. Tsai, M. Tewari, T. Minko, D. E. Discher, *Nat. Nanotechnol.* **2007**, *2*, 249.
[24] I. W. Hamley, *Angew. Chem., Int. Ed.* **2014**, *53*, 6866.
[25] A. B. Seabra, N. Durán, *Peptides* **2013**, *39*, 47.
[26] S. C. Larnaudie, J. Sanchis, T.-H. Nguyen, R. Peltier, S. Catrouillet, J. C. Brendel, C. J. H. Porter, K. A. Jolliffe, S. Perrier, *Biomaterials* **2018**, *178*, 570.
[27] L. Lei, Z. Xu, X. Hu, Y. Lai, J. Xu, B. Hou, Y. Wang, H. Yu, Y. Tian, W. Zhang, *Small* **2019**, *15*, 1900157.
[28] H. Jin, Y. H. Ding, M. Wang, Y. Song, Z. Liao, C. J. Newcomb, X. Wu, X. Q. Tang, Z. Li, Y. Lin, F. Yan, T. Jian, P. Mu, C. L. Chen, *Nat. Commun.* **2018**, *9*, 270.
[29] R. N. Zuckermann, J. M. Kerr, S. B. H. Kent, W. H. Moos, *J. Am. Chem. Soc.* **1992**, *114*, 10646.
[30] P. S. Low, W. A. Henne, D. D. Doorneweerd, *Acc. Chem. Res.* **2008**, *41*, 120.
[31] W. R. Gray, *Methods Enzymol.* **1972**, *25*, 121.
[32] J. Liu, Y. Yang, W. Zhu, X. Yi, Z. Dong, X. Xu, M. Chen, K. Yang, G. Lu, L. Jiang, Z. Liu, *Biomaterials* **2016**, *97*, 1.
[33] M. A. Castriciano, A. Romeo, N. Angelini, N. Micali, A. Longo, A. Mazzaglia, L. M. Scolaro, *Macromolecules* **2006**, *39*, 5489.
[34] C. Harding, *J. Cell Biol.* **1983**, *97*, 329.
[35] H. Wang, Z. Feng, D. Wu, K. J. Fritzsching, M. Rigney, J. Zhou, Y. Jiang, K. Schmidt-Rohr, B. Xu, *J. Am. Chem. Soc.* **2016**, *138*, 10758.
[36] J. Adler, I. Parmryd, *Cytometry, Part A* **2010**, *77A*, 733.
[37] M. A. Rajora, J. W. H. Lou, G. Zheng, *Chem. Soc. Rev.* **2017**, *46*, 6433.
[38] D. Bechet, P. Couleaud, C. Frochot, M.-L. Viriot, F. Guillemin, M. Barberi-Heyob, *Trends Biotechnol.* **2008**, *26*, 612.
[39] S. S. Lucky, K. C. Soo, Y. Zhang, *Chem. Rev.* **2015**, *115*, 1990.
[40] J. Li, A. Wang, L. Zhao, Q. Dong, M. Wang, H. Xu, X. Yan, S. Bai, *ACS Appl. Mater. Interfaces* **2018**, *10*, 28420.
[41] E. R. Stadtman, B. S. Berlett, *Chem. Res. Toxicol.* **1997**, *10*, 485.
[42] H. Wang, Z. Feng, Y. Wang, R. Zhou, Z. Yang, B. Xu, *J. Am. Chem. Soc.* **2016**, *138*, 16046.
[43] S. J. Riedl, Y. Shi, *Nat. Rev. Mol. Cell Biol.* **2004**, *5*, 897.
[44] X. Liu, H. Zou, C. Slaughter, X. Wang, *Cell* **1997**, *89*, 175.
[45] M. C. DeRosa, R. J. Crutchley, *Coord. Chem. Rev.* **2002**, *233–234*, 351.